Vertical distribution of the different types of aerosols in the stratosphere: Detection of solid particles and analysis of their spatial variability

Jean-Baptiste Renard, C. Brogniez, Gwenaël Berthet, Q. Bourgeois, B. Gaubicher, M. Chartier, J.Y. Balois, C. Verwaerde, F. Auriol, P. François, et al.

Vertical distribution of the different types of aerosols in the stratosphere: Detection of solid particles and analysis of their spatial variability

Jean-Baptiste Renard,[1] Colette Brogniez,[2] Gwenaël Berthet,[1] Quentin Bourgeois,[3] Bertrand Gaubicher,[1] Michel Chartier,[1] Jean-Yves Balois,[2] Christian Verwaerde,[2] Frédérique Auriol,[2] Philippe Francois,[2] Daniel Daugeron,[1] and Cécile Engrand[4]

Received 18 March 2008; revised 8 July 2008; accepted 15 October 2008; published 5 November 2008.

[1] Stratospheric aerosols play a significant role in stratospheric chemistry. In the past, it was assumed that only liquid droplets are present in the stratosphere. Nevertheless, a few lidar measurements have shown that sudden enhancement of aerosol content in the middle stratosphere could be due to meteoritic debris. Aircraft measurements have shown that solid particles can be found in the lower stratosphere; these particles are mainly soot, but also include some interplanetary material. In order to better document the various characteristics of aerosols in the unperturbed stratosphere (i.e., free of volcanic aerosols), we have performed observations using different balloon-borne instruments (Stratospheric and Tropospheric Aerosol Counter (STAC), Spectroscopie d'Absorption Lunaire pour l'Observation des Minoritaires Ozone et NO_x (SALOMON), and Micro Radiomètre Ballon (MicroRADIBAL)) and also some satellite data (Global ozone monitoring by occultation of stars Envisat (GOMOS-Envisat)). These instruments allow us to obtain the number of particles in different size classes, the wavelength dependence of aerosol extinction, and the radiance of the light scattered by aerosols. Combining all the data together, it appears that significant amounts of particles are ubiquitous in the middle stratosphere, above the canonical sulfate aerosol layer. "Background" interplanetary dusts in low concentration are likely present in the stratosphere. Above 30 km, interplanetary dust and largest grains from meteoroid disintegration dominate. Although the disintegration of meteoroids occurs in the upper stratosphere or in the mesosphere at all latitudes, these solid aerosols can be transported to the polar regions by the general circulation and can descend into the middle and lower stratosphere during winter mesospheric descents. Between about 22 km and 30 km, soot particles contribute to the population of aerosols at all latitudes. These soot, likely originating from biomass burning at all latitudes, could be injected into the lower stratosphere by the pyroconvective effect and can then reach the middle stratosphere perhaps owing to the gravitophotophoresis effect as was theoretically proposed. In the lower unperturbed stratosphere, liquid sulfate aerosols dominate, although soot particles are still present. Local horizontal and vertical enhancements of solid aerosols have sometimes been detected, although their origin is not yet determined. The presence of these solid particles can strongly bias the interpretation of in situ and remote sensing measurements when only the presence of liquid aerosols is assumed. Therefore, a new strategy of measurement will be necessary in the future to better characterize the stratospheric aerosol content free of volcanic particles.

Citation: Renard, J.-B., et al. (2008), Vertical distribution of the different types of aerosols in the stratosphere: Detection of solid particles and analysis of their spatial variability, *J. Geophys. Res.*, *113*, D21303, doi:10.1029/2008JD010150.

1. Introduction

[2] Stratospheric aerosols play a significant role in stratospheric chemistry through heterogeneous reactions with nitrogen and halogen species [e.g., *Hanson et al.*, 1994, 1996], and in climate through radiative transfer [e.g., *Lary et al.*, 1999]. It is then necessary to estimate accurately the total amount of particles, as well as their nature and their size distribution. Although it is currently assumed that

[1] Université d'Orléans, LPCE, CNRS, Orléans, France.
[2] Université des Sciences et Technologies de Lille, LOA, CNRS, Villeneuve d'Ascq, France.
[3] LMCA, EPFL, Lausanne, Switzerland.
[4] CSNSM, CNRS IN2P3, Orsay, France.

0148-0227/08/2008JD010150

liquid droplets composed of a mixture of water and sulfuric acid constitute the main family of aerosols, solid particles (interplanetary dust and soot) are also present below 25 km in the atmosphere free of volcanic particles.

[3] Extensive studies have been performed in the past to determine the physical properties of volcanic particles, in particular after the Mount Pinatubo eruption [e.g., *Russell et al.*, 1996], using various measurement techniques such as remote sensing observations from satellite instruments [e.g., *Hervig and Deshler*, 1998; *Steele et al.*, 1999] and balloon-borne instruments [*Berthet et al.*, 2002], from ground-based Sun photometers [e.g., *Dutton et al.*, 1994] and lidars [e.g., *Jäger et al.*, 1995; *Di Girolamo et al.*, 1996], and such as in situ measurements with balloon-borne particle counters [*Deshler et al.*, 2003]. Combined with previous observations, these studies have provided over tens of years estimates of the trends in stratospheric aerosol content after the volcanic eruptions that occurred during the second part of the twentieth century, and during the recovery of low-level content since the end of the 1990s [e.g., *Bingen et al.*, 2004; *SPARC*, 2006].

[4] On the other hand, over the last 20 years or more only a sparse number of measurements have searched for the presence of solid particles in the stratosphere. The presence of interplanetary dust in the middle stratosphere is expected to be about 10^{-4} particles per cm^3 for particles with equivalent diameter of around 1 μm [*Hunten et al.*, 1980; *Biermann et al.*, 1996]. (Hereafter ''middle stratosphere'' refers to the part of the atmosphere in the 25–40 km altitude range.) This dust is ejected by comets as they approach the Sun but is also produced by asteroid collisions. The Earth's atmosphere encounters daily tens of tons of interplanetary material [*Love and Brownlee*, 1993]; about 70% of the total incoming mass is completely vaporized during the entry in the atmosphere and can then condense into ''smoke'' particles with submicronic size in the upper atmosphere [e.g., *Murphy et al.*, 1998]. Larger particles that survive the atmospheric entry, usually called ''micrometeorites'', having sizes from a few μm to $\sim$500 μm and various chemical compositions can be collected at the Earth surface mainly on ice and snow [*Maurette et al.*, 1991; *VanderWood et al.*, 1996; *Duprat et al.*, 2007], after being transported downward in the atmosphere. The presence of such solid grains in the middle stratosphere, with a size greater than 1 μm, has been recently detected by *Renard et al.* [2005a] using balloon-borne measurements although their contribution to the overall aerosol content is low. Such material is also found in the lower stratosphere, as detected by *Brownlee* [1985], *Cziczo et al.* [2001] and *Curtius et al.* [2005] using airborne instruments. These last authors show that the amount of such particles seems to be larger inside the polar vortex in the lower stratosphere after advection from all latitudes to the higher latitudes by the general circulation, and subsequent downward transport.

[5] Unexpected enhancements of solid aerosol content have been reported from lidar observations in the Arctic during the 2000–2001 winter between altitudes of 25 km and 40 km, with strong spatial and temporal variability over a few days [*Gerding et al.*, 2003]. It has been proposed that they could originate from meteoritic debris after disintegration in the atmosphere or from debris of condensed rocket fuel. *Klekociuk et al.* [2005] observed one enhancement around 30 km using a lidar, which was well identified as coming from the disintegration of a large meteoroid of a few meters in diameter on 3 September 2004 over Antarctica. Layers with a vertical width of several hundred meters have been detected. Taking into account the horizontal speed of the winds, the horizontal extent of the layers was estimated to be smaller than 250 km. The analysis of the depolarization of the lidar signal was in agreement with dust particles of meteoritic material in the micrometer size range.

[6] The presence of soot in the lower stratosphere (below 20 km) was detected more than ten years ago using wire impactors on aircrafts [*Pusechel et al.*, 1992; *Blake and Kato*, 1995; *Strawa et al.*, 1999]. Some of these authors have postulated that the soot could come mainly from aircraft traffic. *Baumgardner et al.* [2004] and *Schwarz et al.* [2006] have estimated the relative amount of soot with respect to liquid aerosols and have estimated the average mass concentrations with airborne instruments using the laser-induced incandescence technique (heating the aerosols to vaporization temperatures). Following the theoretical calculations of *Hendricks et al.* [2004], they concluded that the contribution of aircraft emissions to large-scale soot mass concentration is small; they have thus proposed that the soot must come from ground-based anthropogenic activities and biomass burning. Recently, *Murphy et al.* [2007] have analyzed the composition of single particles in the lower stratosphere. In particular, they have found that soot particles mainly composed of carbon and larger than 0.3 μm can remain for months in the atmosphere. On the other hand, particles originating in the stratosphere from meteoritic material acquired only small amounts of (organic or elemental) carbon having terrestrial origin when they are transported downward to the tropopause. These particles exhibit optical properties that will differ from those of soot; thus meteoritic material might be not confused with soot having a terrestrial origin.

[7] *Baumgardner et al.* [2004] have shown that the soot could be the main population of aerosols in the lower stratosphere for particles having a size greater than 0.3 μm, at least at Arctic latitudes. The soot concentration at midlatitudes detected by both *Baumgardner et al.* [2004] and *Schwarz et al.* [2006] is about 30 times lower than in the Arctic. These measurements indicate a strong spatial variability of soot aerosol content depending on the latitude; nevertheless, it cannot be excluded that the large content measured at high latitude can be due to a misidentification of meteoritic material.

[8] All the previous soot measurements were conducted in the lower stratosphere. Theoretical calculations [*Pusechel et al.*, 2000] have shown that soot could be present in the middle (and even high) stratosphere. This could result from vertical transport owing to the gravitophotophoresis effect [e.g., *Rohatschek*, 1996], induced by the incidence of sunlight on strongly absorbing particles followed by a thermal effect inside them. This transport could take several years. Nevertheless, this theoretical work needs experimental confirmation. This process could seriously affect the validity of the analysis of solid aerosol transport conducted assuming only the usual dynamical processes (general circulation and sedimentation).

[9] The possible permanent presence of soot in the middle stratosphere has not been detected yet. The search

for their presence can be conducted using balloon-borne instruments that can reach altitudes higher than 25 km. Because of the low pressures in the stratosphere and the expected small amount of particles, instruments dedicated only to tropospheric and lower stratospheric observations cannot be used. Hence specific instruments dedicated to stratospheric measurements must be used, such as stratospheric particle counters, radiometers that measure the light scattered by particles, and spectrometers that measure the wavelength dependence of extinction. In addition, some satellite instruments that measure the aerosol extinction can be used, but detection could be limited by the signal-to-noise ratio. All these techniques that use the optical properties of aerosols are difficult to interpret separately, since different kinds of particles with different size distributions can give similar optical responses. Furthermore, the use of a priori hypotheses for the analysis of the raw measurements, which are the refractive index of the particles, the shapes of the particles (commonly assumed to be spherical), and the form of the size distribution (commonly assumed to follow a lognormal law), could lead to unrealistic results [*Renard et al.*, 2002]. Consequently it seems necessary to combine the measurements of these different instruments in order to avoid such a priori hypotheses and then be able to detect unambiguously the presence of solid particles in the stratosphere. This is the aim of this paper. In the following, the term "soot" will refer to all kinds of burned particles that contain carbon whatever their origin.

[10] This paper is the first of a series of papers on the analysis of the content and of the various properties of the background aerosols in the unperturbed stratosphere (that is free of volcanic aerosols), using different measurement techniques. In this first paper, we will consider sparse balloon-borne and satellite measurements obtained during the 2003–2006 period that will allow us to distinguish between the liquid and solid particles from the tropopause to the middle stratosphere in different geophysical conditions, to identify their different optical and physical properties, and to analyze their spatial variability.

2. Instruments and Measurements Used for Middle Stratosphere Aerosol Studies

2.1. Particle Counting

[11] The Stratospheric and Tropospheric Aerosols Counter (STAC) is an instrument that can be mounted onboard various gondolas under stratospheric balloons [*Ovarlez and Ovarlez*, 1995]. This instrument can be operated under the low-pressure conditions encountered in the middle stratosphere, and can detect low number of aerosols, down to about 10^{-4} particles cm^{-3} μm^{-1} [*Renard et al.*, 2005a]. Owing to its large dynamic range, STAC can be operated from the troposphere up to the middle stratosphere (above 30 km). A first version of the instrument was operated from 1994 to 2001. The instrument was then improved to give better accuracy, and this new version has been operated routinely since 2003.

[12] Particles are drawn through a light beam emitted by a laser diode at 780 nm, and the scattered light is received by a photodetector at a scattering angle of 70°. The number concentrations are calculated from the count rate of the photoelectric pulses received. Diameters of the particles are determined from the pulse height and are sorted into six size classes, assuming non absorbing liquid particles composed of a common mixture of water and sulfuric acid with a refractive index of 1.45 [*Bemer et al.*, 1990]. The size classes can be chosen before the flight, in the 0.35–2.0 μm range. The numbers of particles detected in each size class are divided by the width of the size class in order to retrieve the size distribution in cm^{-3} μm^{-1}.

[13] The main difficulty with such an instrument is the pumping device that must work even under the low-pressure conditions encountered in the middle stratosphere. Tests have been conducted in a low-pressure chamber in order to evaluate the functioning of the pumping device. Taking into account the pump efficiency and the noise of the detector, the counting uncertainty is of 60% for aerosol number smaller than 10^{-3} cm^{-3} μm^{-1}, is reduced to 20% for numbers around 10^{-1} cm^{-3} μm^{-1}, and is better than 6% for aerosol number larger than 1 cm^{-3} μm^{-1}. It is obvious that such an instrument cannot provide an accurate retrieval of the size distribution of solid particles having a different refractive index, or including possibly a nonzero value for the imaginary part of the index [*Renard et al.*, 2005a]. Nevertheless, it can be used to detect the presence of such particles, which can be less luminous than liquid droplets, provided enough light is scattered.

[14] Measurements are conducted during balloon ascent, at float altitude, and during the slow descent when possible. A sliding average filter is applied to the vertical profile data in order to minimize the noise, which allows us to identify vertical fluctuations of aerosol content with a resolution greater than 100 m. Furthermore, some measurements can be conducted at the end of the flight during the drop of the gondola. In this case, the vertical resolution in the middle stratosphere is limited to about 1 km because of the fast falling speed, while the resolution in the lower stratosphere and upper troposphere is similar to that during the ascent since the gondola drop is slowed down by the parachutes. A list of the 8 flights conducted at midlatitudes and high latitudes is presented in Table 1.

2.2. Measurement of Extinction Wavelength Dependence

[15] The wavelength dependence of aerosol extinction can be retrieved from the balloon-borne spectrometer, Spectrométrie d'Absorption Lunaire pour l'Observation des Minoritaires Ozone et NOx (SALOMON), in the 400–675 nm range [*Berthet et al.*, 2002]. This instrument uses the Moon as a light source. Observations are mainly conducted during the balloon ascent, when the Moon has a positive elevation above the gondola horizon, allowing a vertical scan of the atmosphere.

[16] A reference spectrum is obtained at float altitude (between 30 and 40 km) where the air mass factor of the line of sight reaches its minimum value. The atmospheric transmission spectra are obtained by dividing the spectra recorded during the ascent with this reference spectrum. The Rayleigh contribution is calculated using temperature and pressure measurements obtained during the ascent (using onboard Vaisala sensors), and the contributions of ozone, NO_2, NO_3, and OClO at high latitudes, are searched for by a Differential Optical Absorption Spectroscopy (DOAS) method [e.g., *Platt*, 1994]. The contribution of these species

Table 1. List of Measurements[a]

Instrument	Method of Measurements	Date	Location
STAC	counting	16 Jan. 2003	KRN (inside vortex)
STAC	counting	5 March 2004	KRN (outside vortex)
MicroRADIBAL	radiance	8 March 2004	KRN (outside vortex)
STAC	counting	8 March 2004	KRN (outside vortex)
STAC	counting	11 March 2004	KRN (outside vortex)
STAC	counting	9 June 2004	ASA
STAC	counting	7 Oct. 2005	ASA
SALOMON	extinction	16 Jan. 2006	KRN (inside vortex)
STAC	counting	16 Jan. 2006	KRN (inside vortex)
GOMOS (Envisat)	extinction	16 Jan. 2006	KRN (inside vortex)
STAC	counting	20 Jan. 2006	KRN (inside vortex)
GOMOS (Envisat)	extinction	20 Jan. 2006	KRN (inside vortex)

[a]KRN, Kiruna (northern Sweden); ASA, Aire sur l'Adour (southwest of France).

and of the Rayleigh scattering is then subtracted from the optical depth spectra. The resulting residual spectra correspond to the wavelength dependence of the optical depth of aerosols, and are fitted by a fourth-order polynomial. Such a polynomial is well suited to reproduce the nonmonotonous and small color effects present in the spectra. The vertical profiles of aerosol extinction are then obtained every 25 nm after performing a spatial inversion using a least squares fit method. Although the error on extinction values slightly varies from one altitude to another, it is found to be of about 1×10^{-4} km^{-1} at all altitudes for all wavelengths. In fact, this value is the error on the aerosol extinction relatively to the aerosol extinction values obtained at float. If aerosols are present above the float altitude, the absolute value of aerosol extinction can be underestimated, then the true error can be larger. Also, some changes in the shape of the aerosol extinction spectra at high altitude could more or less distort the transmission spectra at lower altitude [*Renard et al.*, 2002].

[17] The flight of SALOMON considered here occurred inside the Northern polar vortex from Kiruna (Northern Sweden) on 16 January 2006 (Table 1). This flight was optimal for aerosol studies in the middle stratosphere, owing to a float altitude of 35 km. In addition to measurements performed during the ascent, some measurements were conducted around the float altitude while the balloon was carried along by the wind. Such conditions allowed us to perform a horizontal scan of the optical depth of aerosols above the balloon float altitude. STAC was mounted on the gondola, in order to tentatively correlate the aerosol content and its spatial variability derived from both counting and extinction observations.

[18] This flight was conducted during one of the validation campaigns of the Global Ozone Monitoring by Occultation of Stars (GOMOS) instrument onboard the Envisat satellite. The GOMOS measurements can be used for the present work on aerosols. GOMOS is a UV-visible spectrometer using stars as light sources, dedicated to the retrieval of the vertical profiles of ozone, NO_2, NO_3, and of the wavelength dependence of aerosol extinction [*Bertaux et al.*, 2004; *Kyrölä et al.*, 2004]. In fact, aerosol retrieval from GOMOS is difficult. The available vertical profiles are noisy, and the wavelength dependence of aerosol extinction can be estimated only when the brightest stars are observed. For the validation exercise, *Renard et al.* [2008] have proposed an improved algorithm (hereafter called the "LPCE processor") in order to retrieve more accurately the wavelength dependence of aerosol extinction in the 400–675 nm spectral range, from the tropopause up to an altitude of 45–50 km. This algorithm is similar to the one used for SALOMON and gives similar errors bars (about 1×10^{-4} km^{-1} at all altitudes for all wavelengths). In the following, GOMOS vertical profiles obtained with the LPCE processor will be considered.

[19] On 16 January 2006, the collocation criteria between GOMOS and SALOMON measurements were less than 400 km and less than 1 h, and observations were conducted under the same geophysical conditions (inside the polar vortex). GOMOS had observed the brightest star of the sky, Sirius, giving high signal-to-noise ratios. So, a direct comparison of the vertical profiles of aerosols extinction in the middle stratosphere was conducted, as well as an estimation of the aerosol content and of the spectral dependence of the extinction in the upper stratosphere. The same conditions for GOMOS observations occurred during another flight of STAC on 20 January 2006, also inside the polar vortex (Table 1). This second case-study could help to study the variability of aerosol content 4 days apart.

2.3. Radiance Measurements

[20] The last instrument used in this study for the detection of aerosols is the radiometer Micro Radiomètre Ballon (MicroRADIBAL) flown on stratospheric balloons. The measurements are performed in 5 channels in the near infrared at 730 nm, 865 nm, 1000 nm, 1270 nm and 1620 nm [*Brogniez et al.*, 2003]. The radiometer collects sunlight scattered by the atmosphere (gas and particles). Absolute calibration performed in the laboratory enables radiances of the scattered sunlight to be inferred. Owing to the rotation of the gondola around its vertical axis, the observations are performed in various directions in a horizontal plane. The scattering angle corresponding to each line of sight is deduced using a magnetometer onboard the gondola.

[21] In the MicroRADIBAL analysis, we consider the radiance L normalized to the solar irradiance E outside the Earth's atmosphere, called the reflectance ρ,

$$\rho(\theta) = \frac{\pi L(\theta)}{E}, \tag{1}$$

where θ is the scattering angle. The normalized radiances are then studied in the form of reflectance diagrams (i.e., reflectance versus scattering angle for given altitude ranges).

[22] Measurements are conducted during the slow descent of the balloon. In order to reduce the impact of the small oscillations of the gondola, the diagrams have been smoothed over 5° of scattering angle and have been averaged over about 500 m of altitude. The diagrams are nearly symmetric with respect to the solar incident plane; thus for the retrievals we have averaged the measurements obtained for positive and negative scattering angles.

[23] To analyze the measurements, in the single scattering approximation the reflectance in each channel is expressed as follows [*Santer et al.*, 1988]:

$$\rho_\lambda(\theta) = \frac{t_\lambda(\theta)}{4}\left\{\delta_{\lambda,aer}\left(p_{\lambda,aer}(\theta) + 2\rho_{\lambda,g}\sin\varepsilon_s\right) + \delta_{\lambda,Rayl}\left(p_{Rayl}(\theta) + 2\rho_{\lambda,g}\sin\varepsilon_s\right)\right\}, \quad (2)$$

where t is the atmospheric transmission from the sun to the detectors, δ is the slant optical depth, p is the scattering phase function, $\rho_{\lambda,g}$ is the reflectance of the atmosphere or ground below the balloon and ε_s is solar elevation. The subscripts "aer" and "Rayl" refer to aerosols and Rayleigh respectively. The Rayleigh slant optical depth is derived from the temperature and pressure profiles that are available from the PTU sounding performed at the same time and close to the balloon trajectory. Estimation of the surface reflectance $\rho_{\lambda,g}$ has been obtained by using a reflectance meter onboard the gondola.

[24] The Rayleigh and the surface contributions are removed from the measured reflectance to derive a term called the "corrected reflectance",

$$\rho_\lambda^{corr}(\theta) = \frac{\rho_\lambda(\theta)}{t_\lambda(\theta)} - \frac{\delta_{\lambda,Rayl}}{4}\left(p_{Rayl}(\theta) + 2\rho_{\lambda,g}\sin\varepsilon_s\right) \quad (3)$$

which corresponds to the aerosol signature

$$\rho_\lambda^{\mathrm{corr}}(\theta) = \frac{\delta_{\lambda,\mathrm{aer}}}{4}\left(p_{\lambda,\mathrm{aer}}(\theta) + 2\rho_{\lambda,\mathrm{g}}\sin\varepsilon_{\mathrm{s}}\right). \quad (4)$$

Thus the measured corrected reflectance diagrams (equation (3)) can be compared to corrected reflectances computed with equation (4) for various computed phase functions (for example using Mie theory) in order to characterize the nature and/or the size distribution of the aerosols [*Herman et al.*, 1986].

[25] MicroRADIBAL performed measurements on 8 March 2004 from Kiruna during a GOMOS-Envisat validation campaign, outside the polar vortex (Table 1). Measurements were performed during the slow descent of the balloon from an altitude of 27 km down to 19 km. The analysis of the raw measurements shows that the noise of the data increased with increasing wavelength; conversely the Rayleigh scattering is stronger at shorter wavelengths. As a consequence the signal-to-noise ratio was best over a wide altitude range only for the 865 nm channel.

[26] STAC was also mounted on the MicroRADIBAL gondola during this flight. Unfortunately, GOMOS observed only a weak magnitude star on this date. Thus, the wavelength dependence of aerosol extinction cannot be accurately retrieved; only the total content of aerosols was estimated, but was not accurate enough for the present analysis in the upper and middle stratosphere [*Renard et al.*, 2008].

3. Analysis of Counting Measurements

[27] The vertical profiles of size distribution obtained by STAC are presented in Figure 1. The chosen size classes are similar from the second to the seventh flight (0.35–0.4 μm, 0.4–0.5 μm, 0.5–0.6 μm, 0.6–0.7 μm, 0.7–0.9 μm, 0.9–2.0 μm). Only small changes were made to the middle size classes compared to the first flight (0.5–0.55 μm and 0.55–0.7 μm). On the other hand, the size class ranges were different for the last flight: the 0.35–0.40 μm range was removed, and the large width size class was subdivided in two smaller width size classes (0.9–1.3 μm and 1.3–2.0 μm). No data was available during the descent of this last flight.

[28] All the measurements show that large amounts of aerosols are present in the middle stratosphere, sometimes with a content similar to that around the tropopause. This result is in contradiction with the current assumption that the background aerosol content is maximum below 20 km and then decreases with increasing altitude. The profiles exhibit strong variability from one flight to another. One can postulate that these differences could arise from problems in the collecting device or contamination by the balloon, thus a careful analysis of the measurements has been conducted. Sometimes more aerosols are detected during descent than during ascent, but other times it is the reverse. Then there is no correlation between the conditions under which the measurements are made and the detected content. The analysis of the geometry of the ascent and of the descent, which is inclined (as explained below) showed that the air masses crossed by the balloon and STAC are different, thus preventing the pumping of particles released by the balloon. In addition the measurements performed during the sparse releases of ballast during the flights were removed. All these facts indicate that this variability in the aerosol content is

Figure 1. STAC measurements. Thick lines: measurements during the gondola ascent; thin lines: measurements during the gondola descent. KRN, Kiruna (Northern Sweden); ASA, Aire sur l'Adour (southwest of France). Conditions of measurements are given in Table 1. The aerosols are assigned to the different size classes assuming liquid particles with a refractive index of 1.45. The counting uncertainty is of 60% for aerosol numbers smaller than 10^{-3} cm^{-3} μm^{-1}, is reduced to 20% for numbers around 10^{-1} cm^{-3} μm^{-1}, and is better than 6% for numbers larger than 1 cm^{-3} μm^{-1}. Note that the size classes for the 16 January 2003 and the 20 January 2006 flights are different from those for the other flights. STAC was mounted on the MicroRADIBAL gondola for the 8 March 2004 flight and on the SALOMON gondola for the 16 January 2006 flight.

not due to a technical problem or contamination, but seems to be real.

[29] On 9 June 2004, 7 October 2005 and 16 January 2006, at midlatitudes and high latitudes, some striking structures appear around 25 km, with three consecutive layers of a few hundred meters in width with a large increase in aerosol content. Taking into account only dynamical causes, it seems difficult to explain why three

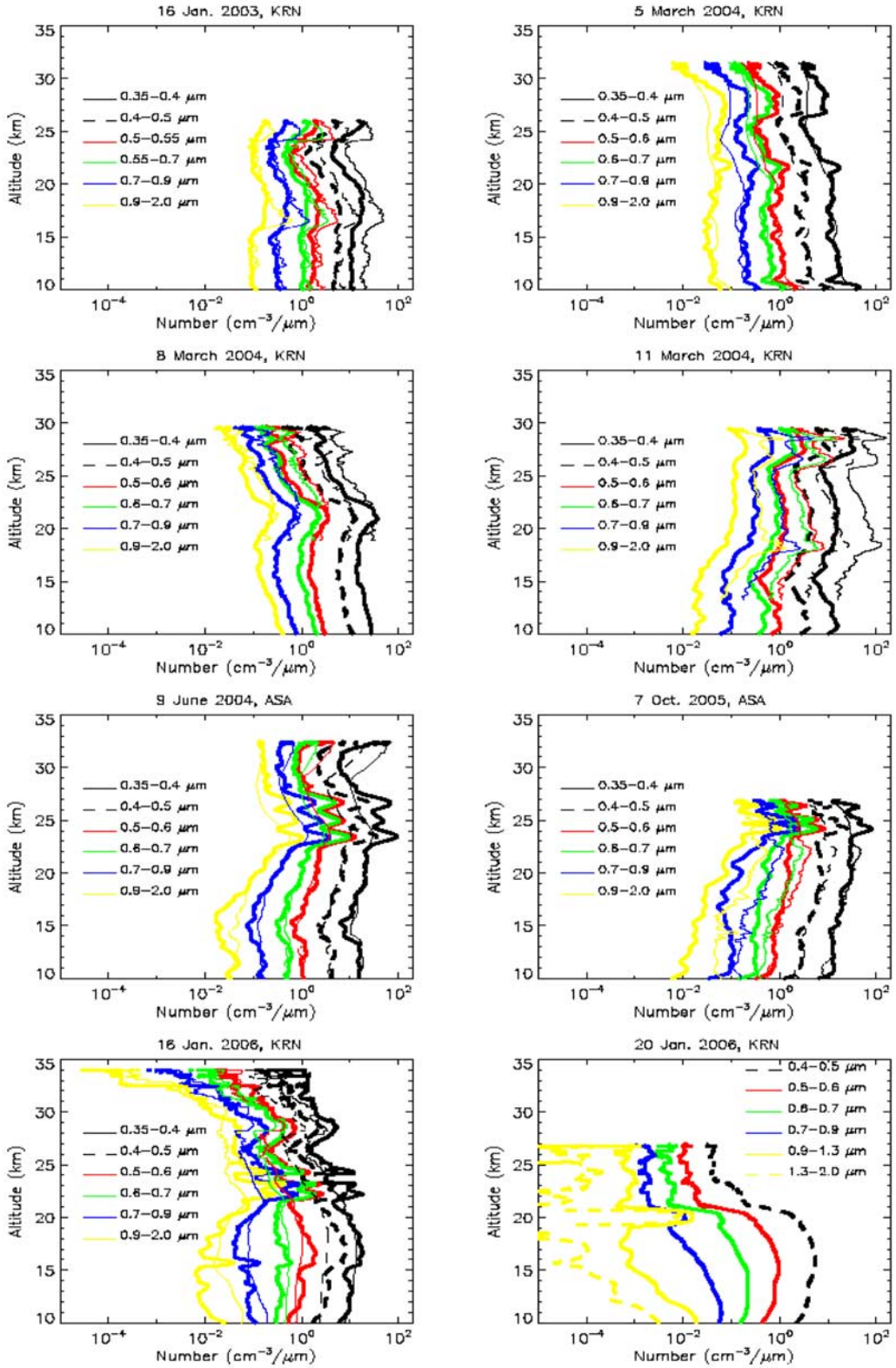

Figure 1

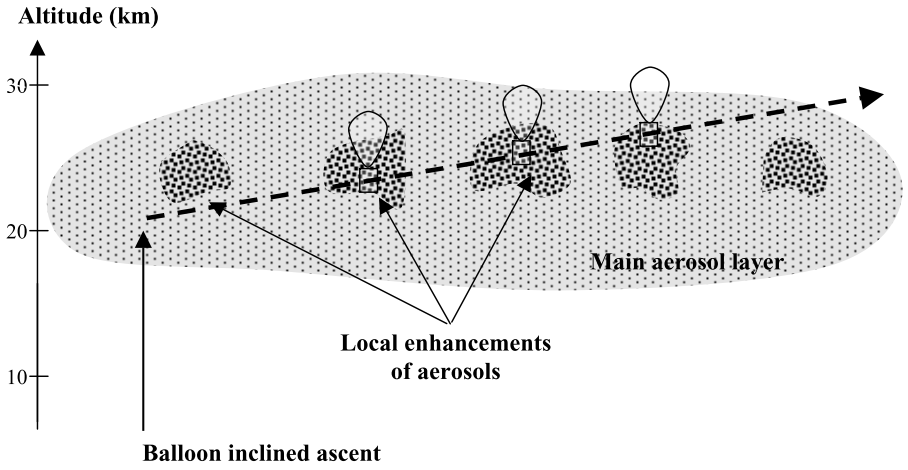

Figure 2. Geometry of measurements during some ascents of the stratospheric balloons. The presence of local enhancements around 25 km crossed obliquely during the slant ascent of the gondola (represented by the dashed line) can produce three consecutive artificial thin layers on the STAC profiles.

enhancements, but no more, are present. However, this can be explained by the geometrical configuration of the balloon's ascent trajectory. During these flights, strong horizontal winds of up to tens of meters per second were sometimes encountered during the ascent, while the vertical ascent speed of the balloon was between 3 and 5 m s^{-1}. Thus, measurements were not conducted during a purely vertical ascent, but during an inclined ascent, with an angle up to 80° with respect to the vertical. Let us assume that strong local aerosol enhancements having horizontal and vertical thicknesses of a few km are sometimes superimposed on the background aerosol layer at similar altitudes (around 25 km). The balloon can cross different enhancements successively at the bottom, middle and top during the inclined ascent, as shown in Figure 2. The altitude of the balloon is higher by a few hundred meters when the balloon leaves the enhancement than when it enters, thus producing artificially thin peaks in the profiles. Such ''artificial'' vertical structures were not observed in the profiles during the fast descents of the gondola on 9 June 2004 and on 16 January 2006 that were close to the vertical, since gravity acts more strongly on the gondola than the winds. Also, no enhancements were observed during the slow descent of STAC on 7 October 2005 that was performed only a few tens of kilometers apart from the ascent trajectory. Taking into account the position of the ascending gondola obtained from an onboard GPS, the size of local enhancements can be estimated. For the three STAC flights considered here, the vertical thickness is on the order of 4 km and the horizontal extent is in the 2–8 km range, highlighting the rather local character of these enhancements. *Berthet et al.* [2007] have shown that the stratosphere was highly perturbed during the 16 January 2006 flight, with strong and sharp intrusions of midlatitude air in the polar vortex at various altitudes. Air masses with different amounts of aerosols and having different origins could explain the strong variability in this STAC profile. Strong dynamical perturbations could be proposed as an explanation for the other STAC flights where some strong large-scale variability was detected. The analyses of the PV maps available at the time of the measurements are in favor with this hypothesis although no definitive conclusions can be given.

[30] At present, it is not possible to distinguish between liquid and solid particles in the STAC measurements, except for the 20 January 2006 flight. Estimates of the aerosol number of the largest particles, with diameter greater than 1 μm, can be made by considering the size class of 1.3–2.0 μm. Their number appears to be almost constant above 15 km, at around 10^{-4} particles cm^{-3} μm^{-1}, if one excludes the strong local enhancement around 20 km that is probably due to a small liquid Polar Stratospheric Cloud (this is consistent with the temperature measurements showing the possibility of PSC occurrence). This value of number is similar to a previous estimate by *Renard et al.* [2005a] using a STAC prototype that was launched on 22 October 2001 at midlatitudes. The authors have shown that this number is in agreement with theoretical calculations for interplanetary dust particles with equivalent diameter of 1 μm or larger [*Hunten et al.*, 1980; *Murphy et al.*, 1998], at least for those that can reach the Earth's surface [*Maurette et al.*, 1991; *VanderWood et al.*, 1996]. The 20 January 2006 measurements are thus believed to be representative of interplanetary dust particles. The diameters of such large solid particles, which can have irregular shape, could differ significantly from those determined from STAC measurements assuming spherical liquid particles. Thus, only an estimate of the amount can be derived without considering their size. Also, it is obvious that this good evidence of the presence of interplanetary dust particles must be confirmed by in situ sample of these particles and their analysis in laboratory.

[31] *Renard et al.* [2002] have shown that, assuming liquid droplets, the size distribution of stratospheric aerosols does not follow a lognormal law, probably because of the possible presence of different types of particles affecting the measurements. It seems then unrealistic to be able to propose another simple mathematical law to describe the size distribution of aerosols using only the 6 size classes determined by STAC measurements. Nevertheless, the behavior of the profiles obtained for the different classes can

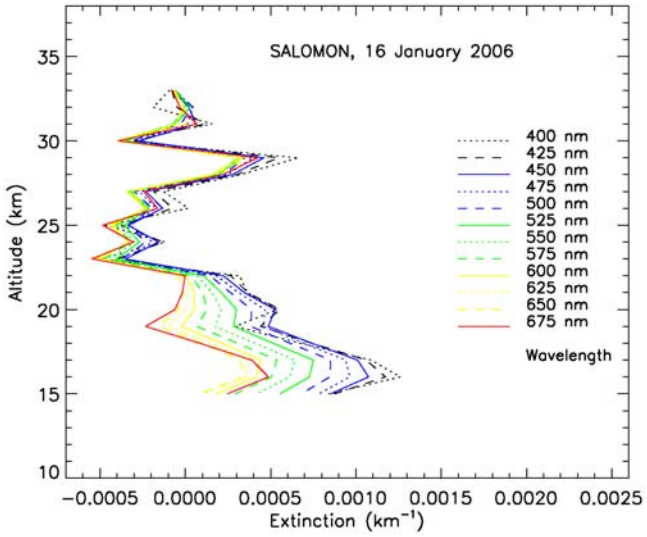

Figure 3. Wavelength dependence of aerosol extinction measured by SALOMON on 16 January 2006 inside the northern polar vortex. For clarity, the error bars (about 1×10^{-4} at each wavelength) are omitted. The negative values above 22 km can appear during the spatial inversion if the contribution of aerosols is not equal to zero in the reference spectrum and/or if local enhancements are present around the float altitude.

be intercompared in order to qualitatively estimate the evolution of the size distribution. For increasing altitudes, it appears that the profiles are in contradiction with the common assumption that the number of largest liquid aerosols decreases continuously with respect to the number of smallest aerosols. We could conclude that different characteristics of aerosols of submicronic size, varying with altitude, were detected by STAC in the lower and middle stratosphere. Since they probably have different refractive indices, the assignation of these particles to the various class sizes can be biased. Other measurement techniques are then needed to tentatively determine the different nature of these particles.

4. Analysis of Extinction Measurements

4.1. SALOMON Observations

[32] Figure 3 presents the wavelength dependence of extinction obtained by SALOMON on 16 January 2006 inside the polar vortex, using measurements obtained during the balloon ascent (with a Moon elevation from +7° to +18°). It must be noted that if a local enhancement of aerosols having different extinction spectra is present above the float altitude of the balloon (34 km), the retrieved wavelength dependence of extinction at each altitude is relative to the extinction of the high-altitude particles, and could differ from the absolute spectral dependence of the extinction.

[33] The SALOMON profile exhibits some negative values on different parts of the profile. Such negative values can appear during spatial inversion if the contribution of aerosols is not equal to zero in the reference spectrum and/or if local enhancements are present around the float altitude (34 km). It is therefore possible to conclude that, during this flight, aerosols are present above 35 km and exhibit a strong vertical variability. The SALOMON measurements conducted at float and during the slow descent from 34 km to 27 km, with a Moon elevation increasing from 18° to 26°, could help to better document the origin of these aerosols. With such a Moon elevation, the line of sight is short and can be very sensitive to local enhancements of aerosol content at the gondola altitude and above. Figure 4 presents the aerosol slant optical depths above the gondola altitude obtained by SALOMON and averaged over the 400–675 nm range, compared to the simultaneous in situ STAC measurements for the smallest particles. (We have used the averaged extinction for clarity reasons, since no additional useful information can be derived when plotting all the wavelengths). Four enhancements were detected by SALOMON with gondola altitudes around 33 km, 31 km, 30 km and 28 km. The first two peaks are detected only by SALOMON; thus the enhancements are above the gondola altitude. The two last peaks were detected both by SALOMON and STAC, so the enhancements are located around the altitude of the gondola.

[34] As stated above, SALOMON also detects the contributions of some atmospheric species. Figure 5 presents the slant column amount of OClO obtained simultaneously with the aerosol optical depth for lines of sight with positive elevation. Such geometry of measurements allows us to only detect the slant columns of the species and aerosol above the float altitude of the instrument. OClO and aerosol variability appear strongly correlated on Figure 5. On the other hand, as shown by *Berthet et al.* [2007], the OClO and

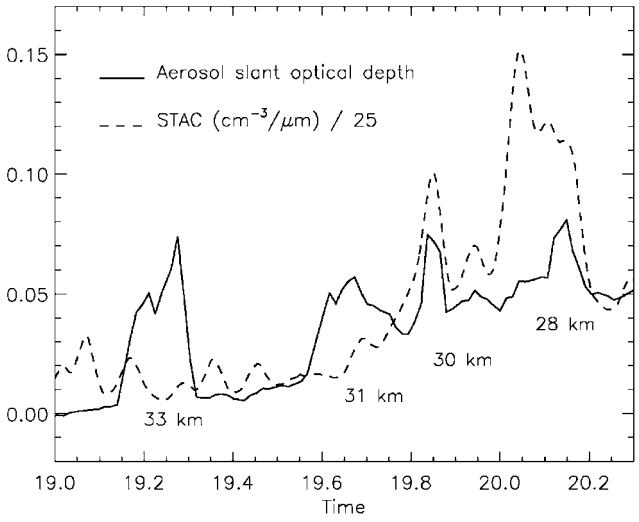

Figure 4. Aerosol slant optical depths (slant column above the gondola altitude) obtained by SALOMON and averaged over the 400- to 675-nm range, compared to the STAC number for the smallest particles in the 0.35 to 0.4-μm size class range divided by 25 to be plotted on the same y scale. The observations were conducted during a slow descent of the gondola from 34 km to 27 km on 16 January 2006. The altitude of the gondola is indicated below the main enhancements. The absolute error for optical depth is 1×10^{-4}, and the uncertainty for STAC measurements is less than 5%.

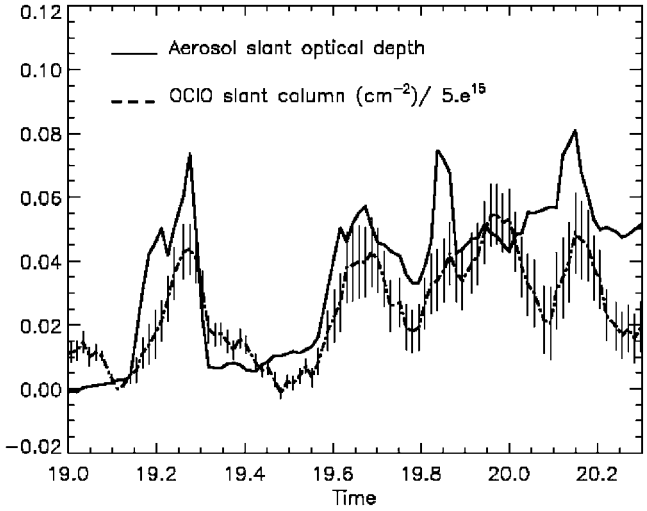

Figure 5. Comparison between aerosol slant optical depths averaged in the 400- to 675-nm range and the OClO slant column above the gondola altitude, obtained by SALOMON on 16 January 2006.

NO_2 slant columns are strongly anticorrelated. The polar vortex was highly perturbed at these altitudes in mid-January 2006, with intrusions of air masses coming from midlatitudes. Such air masses are free of OClO and contain large amounts of NO_2; in contrast, the air masses containing OClO have a polar vortex origin. Thus, as can be derived from Figure 5, only the polar air masses contain the high-altitude strong local enhancements of aerosols. One possible explanation is that such enhancements are typical of a larger content of solid particles coming from the interplanetary medium and/or from some meteoritic disintegration events, such as those observed in the past [*Gerding et al.*, 2003], then being transported from all latitudes to the polar latitudes by the general circulation and finally being downward transported via the mesospheric descent occurring in the polar vortex. Sensitivity calculations on the absorption by solid particles show that extinction measurements are more sensitive to a small amount of large dust grains than large amount of small "smoke" particles, so SALOMON has probably detected the presence of the largest dust grains.

[35] The most obvious vertical structure in the SALOMON vertical profile (obtained during the ascent) is a strong enhancement at altitudes of 28−29 km (Figure 3). This structure is well correlated with the enhancement detected at this altitude by STAC during both ascent and descent. Thus, this layer has a large horizontal extent. Taking into account the trajectory of the flight, we can estimate that the width is at least 120 km, and that this layer strongly differs from the few-kilometers-wide local enhancements detected by STAC at altitudes around 25 km (as discussed in section 3). We can propose that this layer is also possibly composed of the dust grains mentioned above and downward transported.

[36] The wavelength dependence measured by SALOMON (Figure 3) exhibits two different types of behavior. Below 22 km, the extinction is greater in the blue than in the red, with an almost monotonous decrease with increasing wavelength. This is typical of the extinction produced by small droplets, such as the liquid sulfate aerosols; it is well known that such particles, composed of a mixture of water and sulfuric acid, are the main aerosol population in the lower stratosphere as shown unambiguously by the in situ aircraft measurements presented in the introduction of the paper. Above 22 km, the extinction shows almost no wavelength dependence (i.e., similar values at all wavelengths), taking into account the error bars of 1×10^{-4} km^{-1}. After performing a large number of computations using Mie theory for scattering by spherical particles, we can conclude that such dependence cannot be reproduced by liquid aerosols with the submicronic sizes detected by STAC. On the other hand, micronic solid particles can produce constant extinction. Among the candidates can be soot particles, since laboratory measurements of their optical properties show that they exhibit such constant extinction behavior [*Renard et al.*, 2001].

[37] It is necessary to confirm by other observations that the wavelength dependence detected by SALOMON is real, that soot could be present in the population of aerosol above 22 km and that higher-altitude enhancements could be due to solid extraterrestrial particles. This can be done using satellite data that enable us to detect aerosols in the stratosphere.

4.2. Gomos Observations

[38] The main advantage of using satellite data compared to balloon-borne measurements is that the reference spectrum is really obtained outside the atmosphere. Then the absolute value of aerosol extinction can be obtained, as well as its true wavelength dependence. On the other hand, the short exposure time of satellite detectors (0.5 s in case of GOMOS, to be compared to few tens of second for SALOMON) combined with the fast motion of the satellite limits the accuracy of the retrieved profiles. Furthermore, the length of the line of sight is about 10 times greater with GOMOS than with SALOMON, thus it integrates the possible local fluctuations of aerosol content and smoothes the vertical profiles.

[39] The two GOMOS profiles from the 16 and 20 January measurements close to Kiruna that have been considered here were obtained with the "LPCE processor" and are shown in Figures 6 and 7. In the lower stratosphere, the 16 January GOMOS extinctions (Figure 6) are larger than those detected by SALOMON. But if the SALOMON values are shifted by 5×10^{-4} km^{-1}, which corresponds to the strongest negative values obtained because of the presence of aerosols above the balloon float altitude (see Figure 3), the resulting extinctions are close to those of GOMOS.

[40] The SALOMON and GOMOS wavelength dependences exhibit similar global behavior, with a strong change in the wavelength dependence around 22 km for SALOMON and around 20 km for GOMOS. This altitude difference could be due to the presence of aerosols above the float altitude that more or less alters the retrieval of the SALOMON spectra, but also due to the 3-km vertical resolution of GOMOS. Nevertheless, the comparison shows that the SALOMON wavelength dependence retrieval is not strongly biased by the contribution of aerosols above the float altitude.

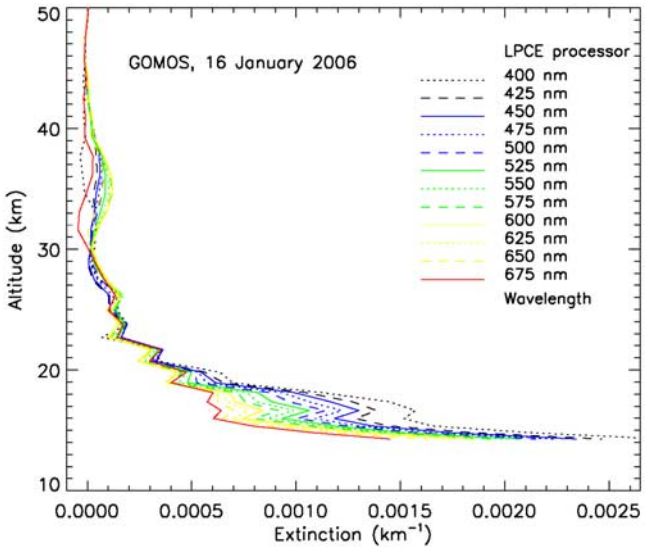

Figure 6. Wavelength dependence of aerosol extinction measured by GOMOS obtained with the "LPCE processor", for 16 January 2006 inside the northern polar vortex. For clarity, the error bars (about 1×10^{-4} km^{-1} at each wavelength) are omitted.

[41] In Figure 6, the GOMOS profile exhibits small vertical variations below the altitude of 26 km that are reminiscent of those detected by SALOMON and STAC at similar altitudes on the same day. The second GOMOS profile obtained four days later (Figure 7) is smoother than the first one in the middle stratosphere, in agreement with the smoother profiles obtained by STAC. Then, this first analysis confirms qualitatively both the spatial and temporal aerosol variability detected by SALOMON and STAC.

[42] Three different vertical regions can be found in the two GOMOS profiles. Above the tropopause and below 21 km, the extinction is stronger in the blue than in the red, which is indicative of the usual small-sized sulfate aerosols. Between 21 and 27–30 km, the extinction is almost constant, thus giving more evidence that soot particles are really present. Finally, above 27–30 km, a small enhancement of aerosol content appears, with nonmonotonous wavelength dependence of extinction and a stronger extinction around the yellow spectral domain. Such spectral dependence has already been observed in the past by SALOMON in the middle stratosphere with flights performed at float altitudes higher than 30 km and cannot be reproduced using Mie theory for liquid droplets [*Renard et al.*, 2005a]. It was interpreted as a color effect produced by interplanetary dust and by the largest solid grains resulting from the meteoritic disintegration (these particles are not the "smoke particles" which exhibit a monotonous wavelength dependence of extinction).

[43] Among the three different types of aerosols that could have been identified, the more surprising result is the possible detection of soot in the middle stratosphere up to an altitude of 30 km. This altitude is above altitudes reached by fire plumes reported previously in several papers [e.g., *Jost et al.*, 2004]. Another measurement technique is necessary to conclude unambiguously on the (permanent?) presence of soot in the middle stratosphere. This can be done using the radiance data of the balloon-borne instrument MicroRADIBAL.

5. Analysis of Radiance Measurements

[44] The reflectance diagrams derived from MicroRADIBAL measurements are very sensitive to the nature of particles that scatter light, thus enabling the type of stratospheric aerosols to be identified. As stated above, the analysis of the radiances requires reference phase functions as input data. They can be calculated for homogeneous liquid particles using Mie theory or for nonspherical (solid) particles randomly oriented using the T-matrix theory [*Mishchenko et al.*, 1996]. In this last frame computer codes have been developed for inhomogeneous particles (coated) [e.g., *Quirantes*, 2005]. It must be noticed that the composition, shape and size distribution of such aerosol populations are not known, so only rough estimates of their optical properties could be available. Thus, laboratory measurements are better suited for retrieving the scattering phase functions of such particles [e.g., *Hovenier et al.*, 2003].

[45] Most of the MicroRADIBAL corrected reflectance diagrams obtained at $\lambda = 865$ nm exhibit an unusual shape: there is a strong decrease in the 15° to 30° scattering angle range and the shape is almost flat for angles larger than 100°. This behavior is similar to the one computed using the scattering phase function for randomly distributed soot particles with various shapes, obtained recently in the laboratory using the LaMP polarimetric nephelometer at $\lambda = 802$ nm [*Renard et al.*, 2005b]. This phase function of soot is very close to the phase function that can be computed using Mie theory for spherical particles having a refractive index of 1.75 + 0.43i, and a monomodal lognormal size distribution with a median diameter of at least 2 μm and a geometric standard deviation $\sigma = 1.42$ (Figure 8). To tentatively explain this agreement, we could propose as a first approximation that the small soot particles with various shapes and randomly oriented can act like large spherical particles when their individual

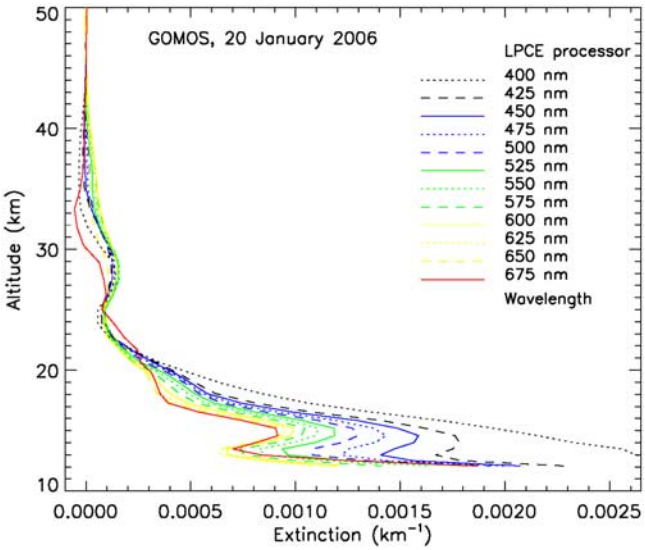

Figure 7. Same as Figure 6, but on 20 January 2006.

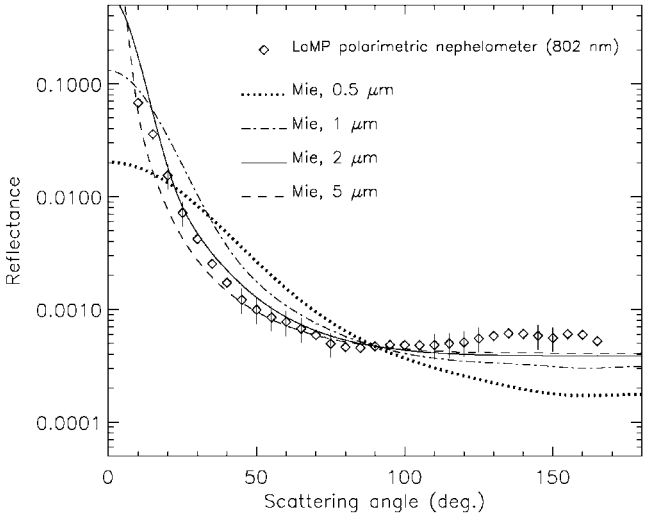

Figure 8. Comparison between soot radiance obtained with the Laboratoire de Météorologie Physique (LaMP) polarimetric nephelometer, and computed phase functions for monomodal lognormal size distributions with different median diameters and a geometric standard deviation σ = 1.42, using Mie scattering theory (spherical particles having a refractive index of 1.75 + 0.43i). The computed curves are rescaled to the Nephelometer curve (in arbitrary units) with respect to its values at 90° scattering angle.

radiance contributions are integrated over the same field of view. Both the laboratory and the MicroRADIBAL instruments observe a large number of particles during the measurements, so we believe that a Mie scattering function with spherical particles of 2 μm median diameter can be used in the following for qualitatively interpreting the stratospheric measurements. It is obvious that such an approximation does not represent the true size and shape distribution of the stratospheric particles and is used here just to simplify the computations in the data reduction.

[46] Since an internal mixing of soot and liquid sulfate can be considered as adequate to represent the coexisting species (long stratospheric residence time of the particles could lead to internally mixed aerosols owing to coagulation and condensation processes), it could be interesting to see if more complex theoretical calculations can be convenient to interpret the MicroRADIBAL measurements. Trials to fit the measurements assuming coated particles (soot core surrounded with a sulfate shell) have been carried out using a code developed by *Quirantes* [2005] (available at http://www.ugr.es/local/aquiran/codigos.htm). These trials have been unsuccessful yet to reproduce the strong increase of scattered light toward small scattering angles and the flat shape at large scattering angles. Thus new theoretical works on the true shape of soot (probably fractal aggregates) and their optical properties are needed; such work is in progress [*Moulin*, 2007], but no usable results are yet available.

[47] Thus in the following we use an idealized description of the aerosols assuming spherical shape and Mie scattering. It must be kept in mind that such assumption is an approximation in order to simplify the analysis of the MicroRADIBAL measurements, and that new analysis must be conducted in the future when more accurate modeling work will be available.

[48] The MicroRADIBAL corrected reflectances are fitted using a bimodal distribution of two Lognormal Distribution components to interpret the measurements in the middle and lower stratosphere. The first mode is composed of soot with the above mentioned refractive index and size distribution parameters, and the second mode consists of liquid sulfuric acid droplets with the usual refractive index. At all altitudes, and after testing a large range of values (median diameter in the 0.05–2 μm range with a step of 0.05 μm and ln(σ) in the 0.05 0.9 range with a step of 0.05), the best fit is obtained for a median diameter of 0.2 μm with σ = 1.42 for the sulfate aerosol mode. The relative concentrations of the 2 modes vary depending on the altitude. The mode of liquid droplets is found in agreement with previous studies on the determination of their size distribution in the stratosphere [e.g., *Berthet et al.*, 2002]. Figures 9 and 10 present the comparison between MicroRADIBAL corrected reflectance diagrams and the computed diagrams at altitudes of 27 km and 19 km. We have also plotted diagrams computed assuming a bimodal distribution with only sulfate aerosols (the two modes also have a median diameter of 0.2 μm and 2 μm and σ = 1.42). At 27 km, the best fit that can reproduce the strong increase of the corrected reflectance toward small scattering angles and the flat shape at large scattering angles is obtained with soot and liquid sulfate particles (solid line). The diagram computed assuming only liquid particles (dashed line) differs strongly from MicroRADIBAL data at such angles. The shape of the corrected reflectance diagrams evolves with decreasing altitudes, becoming less flat at large scattering angles. At 19 km (Figure 10), the computed scattering functions give similar results when a mixing of soot and sulfate particles or when

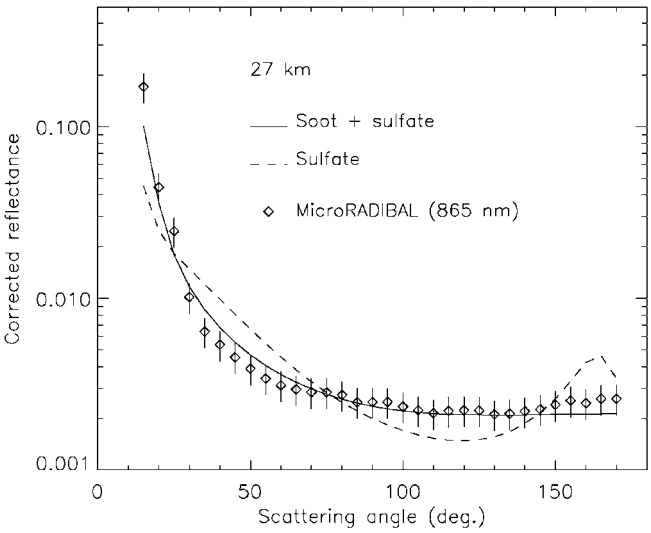

Figure 9. Comparison between MicroRADIBAL corrected reflectance at 27 km and two diagrams computed for bimodal size distributions: (1) with a mode of soot (see Figure 8) and a mode of sulfate particles and (2) with two modes of sulfate particles. The MicroRADIBAL errors are about 10%.

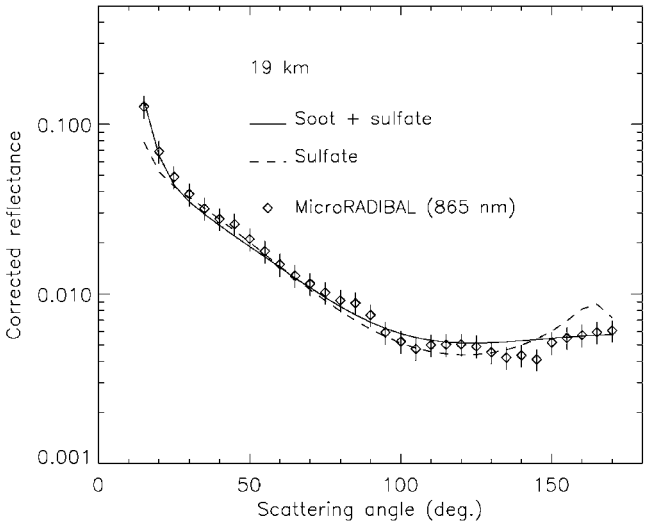

Figure 10. Same as Figure 9, but at 19 km altitude.

only sulfate particles are considered. The analysis of all the measurements shows that the relative concentration of soot decreases and that of sulfate aerosols increases for decreasing altitude. Following the previously mentioned aircraft measurements showing that liquid particles are indeed present at these altitudes, we can consider that an external mixing of soot and sulfates is representative of the lower stratospheric aerosol content.

[49] The aerosol extinction can be estimated from the computed aerosol size distributions that fit the MicroRADIBAL measurements. Such calculations are done in order to link tentatively the MicroRADIBAL results to those obtained from the remote sensing spectrometers. In the middle stratosphere above around 24 km, at least 90% of the total aerosol extinction is due to soot. In the lower stratosphere below 20–21 km the contribution of sulfate aerosols to total extinction is 50% or larger.

[50] Combining the radiance and extinction measurements, it is now possible to conclude that soot particles are likely present in the middle stratosphere at least below 30 km. Although the actual size distribution of these solid particles cannot be retrieved, owing to the assumption of the spherical shape, the measurements qualitatively indicate that, in the unperturbed stratosphere, a large amount of particles different from sulfate aerosols exists above 22–23 km (i.e., above the canonical sulfate aerosol layer), and that these aerosols consist probably of soot.

6. Discussion

6.1. Estimation of the Vertical Evolution of Aerosol Content by Combined Measurements

[51] We can now combine all the previous measurements in order to propose a global view of the vertical distribution of the different types of aerosols in the stratosphere. For this purpose, a "color index" (*CI*) is calculated from GOMOS and SALOMON extinction using the formula

$$CI = (Ext_{400} - Ext_{675}) / \sqrt{\sum_{400}^{675} Ext^2} \ ,$$

where "Ext" means extinction and the number indicates the wavelength in nm.

[52] This color index must be positive when small liquid particles are present, must be close to zero if "large" particles such as soot are present, and could exhibit oscillating values, including negatives values, in the presence of interplanetary material that can have different spectral colors due to the varying nature of their components (silicate, iron metal, ... as detected by *Klekociuk et al.* [2005]).

[53] Figure 11 presents the comparison between the color indices of SALOMON and GOMOS data on 16 January 2006. Qualitatively, the two CI exhibit a similar nonmonotonous behavior with altitude (their difference in absolute values could be due to the accuracy of the measurements and to the residual contribution of upper stratospheric aerosols in the SALOMON measurements).

[54] A scenario could be tentatively proposed to explain these measurements. Below 17–20 km, the size of the liquid sulfate aerosols (superimposed on the permanent background of soot) decreases with increasing altitude. This is in agreement with the fact that the CI increases when the size of the liquid aerosols decreases, as expected from Mie theory. Above 17–20 km, the progressive decrease of the liquid aerosol content (both in size and in concentration) produces the negative gradients on the CI profiles. Above 22 km, soot could be the main population, producing constant CI profiles. Above 30 km, the CI becomes strongly negative in the GOMOS profile (and perhaps at the end of the SALOMON profile), with a minimum value around 40 km. Since soot cannot produce such CI negative values, the best explanation is that an enhanced aerosol layer has been observed at the highest altitudes, which is mainly composed of interplanetary dust and "large" meteoritic debris. Similar CI profile (not shown here) is obtained for GOMOS measurements on 20 January 2006.

6.2. Variability of Aerosol Content in the Stratosphere

[55] As stated above, one high-altitude aerosol enhancement, detected on 3 September 2004 around 30 km by lidar, originates from a well documented disintegration of a large meteoroid [*Klekociuk et al.*, 2005]. Downward transport of similar enhanced layers, from altitudes of 38 km to 26 km, was observed several times during the winter of 2000–2001 [*Gerding et al.*, 2003] without unambiguously identifying their origin. On the other hand, the increases in extinction above 30 km observed by GOMOS in January 2006 are similar to the ones detected on May 1993 at midlatitudes from satellite UV-visible extinction measurements performed by the Solar Occultation Radiometer (ORA) instrument [*Fussen et al.*, 2001] and reported by *Renard et al.* [2005a].

[56] All these instruments have observed transient local enhancements in the middle and upper stratosphere on different dates. They possibly have detected the consequence of the (not always documented) disintegration of smaller meteoroids providing "large grains", which obviously could occur at higher altitudes and more frequently than the stronger event recorded on September 2004. Smaller meteoroids can have a smaller penetration depth in the atmosphere than the largest bodies, so the disintegration could occur higher in the stratosphere. Over a short

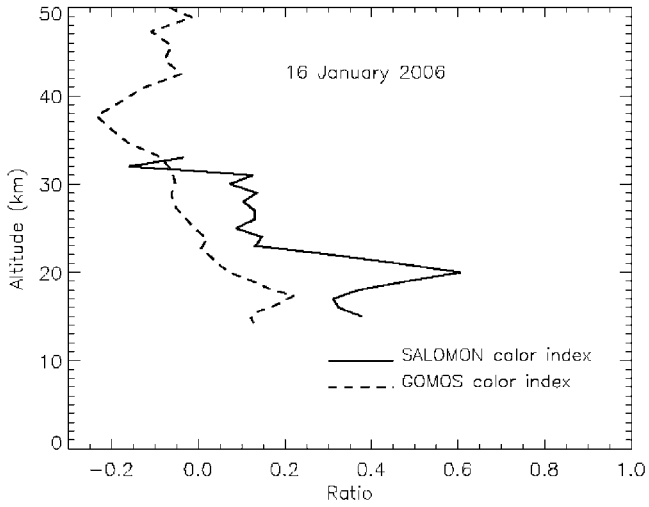

Figure 11. Comparison between color indices of SALOMON and of GOMOS on 16 January 2006 (see text for the description of the color index).

time they can produce local enhancements well above the altitude that can be reached by most of the lidars. Finally, some enhancements could also be the consequence of "shooting stars" storms than can occur occasionally. The limited horizontal sampling as well as the spatial and the temporal coverage of the lidars could have prevented an estimation of the occurrence of such events. Nevertheless, perhaps some lidars could have recorded small enhancements that were not analyzed or overlooked, thus past observations could be reanalyzed in order to search for the vertical structures similar to those presented here.

[57] After formation, the previous enhancements can descend into the middle and lower stratosphere by sedimentation, contributing to the continuous background of the largest particles detected by STAC at all latitudes. They can also be transported to the poles via the general circulation and then transported downward during polar mesospheric descents. They can then be fortuitously detected by balloon and satellite instruments. The detected variability of particle content could be due to the different origins of the air masses sampled by the instruments and having different vertical and horizontal trajectories.

[58] An illustration of the descent of such a layer could be the strongest and the largest enhancement at 29 km detected on 16 January 2006 by SALOMON. Such an enhancement is not present in the GOMOS profile on the same day, which is 400 km distant from the location of the SALOMON observations, but is present on the GOMOS profile on 20 January 2006 owing to the horizontal transport of the layer induced by the rotation of the vortex during the 4 day period, as showed by backward trajectory analyses.

6.3. Origin of Soot

[59] It was assumed in the past that soot resulted from aircraft traffic, since biomass burning soot emitted at the Earth's surface cannot be levitated by the gravitophotophoresis effect that could work only for particles at altitudes higher than 5 km [*Pusechel et al.*, 2000]. Moreover, some previous sparse observations were showing that soot could be in greater concentration near aircraft corridors [*Blake and Kato*, 1995; *Pusechel et al.*, 1997]. Nevertheless, it is difficult to explain both the soot background content and the strong local enhancements well above 20 km that we have observed at various latitudes assuming only an aircraft origin. Two other origins could be proposed. The first one could be the "smoke" particles with submicronic size originating from vaporized interplanetary material, but their amount is probably too low to explain our measurements. The second source is soot coming from biomass burning at various latitudes. Recent observations performed in particular during the fire seasons over North America [*Jost et al.*, 2004; *Ray et al.*, 2004; *Heald et al.*, 2006], have shown that such material was found in the free troposphere. It has been shown that some fires can have sufficient energy to trigger convection, injecting particles also into the upper troposphere and the lower stratosphere [*Fromm and Servranckx*, 2003; *Damoah et al.*, 2006]; this phenomenon is called pyroconvective injection. Then, in agreement with the suggestion made by *Baumgardner et al.* [2004], and *Schwarz et al.* [2006], we can propose that most of the soot is coming from surface sources.

[60] Nevertheless, if these particles detected by the various instruments are indeed biomass burning soot, at this stage the mechanism for transporting them to the middle stratosphere without being mixed with the surrounding air (necessary to explain the strong variability in the measured content) is unknown.

6.4. Consequence of Aerosol Characteristics on the Different Measurement Techniques

[61] The measurements we have analyzed here were obtained during an exceptional time period where the aerosol content is low and free of volcanic particles. All the analyses performed in the past using stratospheric measurements obtained by in situ instruments or by remote sensing satellite or balloon-borne instruments assumed only the presence of liquid particles. This hypothesis was valid because of large amount of volcanic liquid aerosols. Such assumption is too simplistic for the present situation of aerosol content, and the retrieved size distributions and surface area densities that could be inferred from these different measurement methods could be inaccurate [*SPARC*, 2006].

[62] Calculations using the T-matrix theory show that nonspherical particles (homogeneous or not) have an optical response that differs strongly from that of homogeneous spherical droplets. According to several authors [e.g., *Brownlee*, 1985; *Blake and Kato*, 1995] soot and interplanetary dust are not spherical, since they have compact or fractal aggregate shapes, thus the STAC measurements in the middle stratosphere should be reanalyzed assuming soot and dust particles instead of liquid droplets. The raw data should be recalibrated using computations with the refractive index of soot, in order to reevaluate the particle numbers in the various STAC class sizes. Such computations that can be used for interpreting our measurements are not easily feasible at present using available light scattering models.

[63] Nevertheless, such counting measurements can be useful for a qualitative analysis of stratospheric aerosol content, as shown above. The interplanetary dust, which

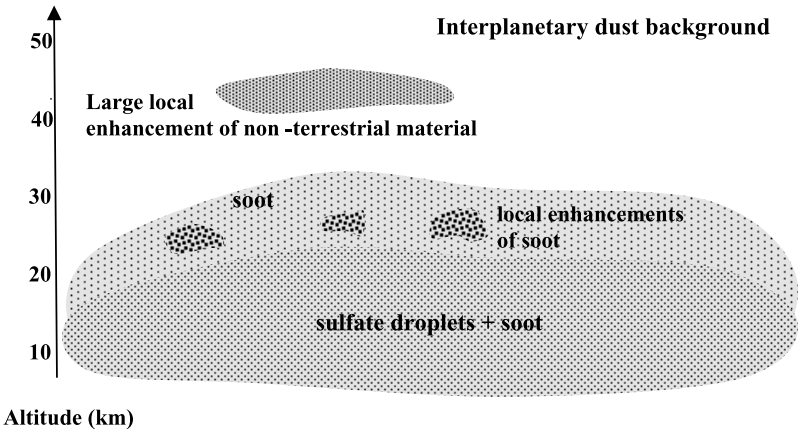

Figure 12. Proposed vertical distribution of the various natures of aerosols in the stratosphere free of volcanic aerosols.

has micron-size diameters or larger (as stated above), would affect only the largest size class in the STAC measurements, thus allowing an estimation of their total number without determining their actual size. If our interpretation is to be confirmed, the submicronic size distributions obtained by the instrument are strongly biased by the presence of soot, but the data can be used for the estimate of the vertical and horizontal variability of the solid aerosol content.

[64] Similar problems are encountered when analyzing the wavelength dependence of aerosol extinction from remote sensing instruments. As stated previously, the presence of interplanetary dust can produce a color effect that cannot be reproduced by Mie theory. Moreover, the almost spectrally flat extinction produced by randomly oriented soot [*Renard et al.*, 2001] does not allow us to solve the inverse problem of retrieving their size distribution in the middle stratosphere. In the lower stratosphere, the extinction produced by soot could be up to 50% of the total extinction in the near infrared, as shown by MicroRADIBAL. Since the soot extinction is spectrally constant, the measured wavelength dependence of extinction, decreasing from the blue domain to the red domain, is due only to liquid droplets. Then their contribution could be tentatively searched for using Mie computations. But one problem remains: what kind of a priori size distribution must be assumed for the computation retrievals? The measurements of *Baumgardner et al.* [2004] in the lower stratosphere show that both size distributions of liquid particles and of soot do not follow a lognormal law or a power law. Therefore it will be impossible to estimate accurately the amount of liquid particles. Thus, the extinction measurements can be useful only to qualitatively point out the changing nature of the population of aerosols with altitude.

[65] We can conclude that all the in situ and remote sensing measurements cannot be used separately to determine the aerosol content. It is then necessary to combine measurements obtained with different techniques to better characterize the various types of aerosols and their vertical distribution. This can be done when different instruments are on the same balloon gondola, and also with correlative satellite extinction measurements. Nevertheless, it seems impossible at present (in unperturbed conditions) to accurately derive the surface area densities of stratospheric aerosols.

7. Conclusions

[66] By using "snap-shot" measurements obtained with different observing techniques, it seems possible to improve knowledge on the true nature of aerosols in the stratosphere free of volcanic aerosols, and to study their variability. Three main results can be pointed out: first, there is a significant amount of aerosols above 22 km, even when volcanic aerosols are absent. Second, the population of aerosols in the 22–30 km altitude range seems to contain soot that could originate from biomass burning, although their true origin cannot be yet unambiguously determined. Third, nonpermanent descending layer(s) of aerosols can be detected at various altitudes in the middle stratosphere, these layers being composed of the largest material coming from disintegration of meteoroids. It is then possible to tentatively propose a description of the aerosol content in the stratosphere free of volcanic aerosols (Figure 12): "Background" interplanetary dusts in low concentration are present in the whole stratosphere; local enhancements with horizontal extension of tens of km sometimes occur in the middle and upper stratosphere, owing to the meteorite disintegration, containing mainly dust grains (and perhaps "smoke particles" which are not detectable by our instruments). Soot could have a large contribution in the middle stratosphere, with sometimes strong kilometer-wide enhancements. Finally, mixtures of soot and sulfate particles are probably also present in the lower stratosphere.

[67] The various characteristics of these different particles will have an implication on the estimation of the radiative transfer effects. Even if the concentration of solid particles is small, they are present over a large altitude range in the middle stratosphere, which leads to a nonnegligible contribution when vertically integrated. For the two January 2006 GOMOS observations considered here, the vertical optical depth at 500 nm can be computed from the vertical profiles. From 13 km to 50 km, the vertical optical depth is about

1×10^{-2} for all the aerosols; the vertical optical depth of soot between 20 and 30 km is about 1×10^{-3}; the vertical optical depth of interplanetary particles between 30 and 50 km is also about 1×10^{-3}. Then the solid particles contribute to about 20% of the total optical depth of stratospheric aerosols.

[68] These solid particles could affect also the stratospheric chemistry through heterogeneous reactions although such reactions have not yet been identified in the laboratory. Since it is not possible at present to derive the size distribution of such particles and their true composition from available optical measurements, strong uncertainties will remain for future chemistry modeling calculations.

[69] Soot ejected from aircraft could probably differ both in shape and in composition from those coming from biomass burning (and from the "smoke" particles). Also, interplanetary grains have different shapes and compositions because of the various natures of their mineral and organic components [*Zolensky et al.*, 1994; *Jessberger*, 1999; *Engrand and Maurette*, 1998]. Then, the in situ and remote sensing measurements that use optical methods will not be useful for distinguishing between these different materials. One of the best methods to determine the composition of the solid particles consists in collecting the particles, and analyzing them in the laboratory. Such collection has been done in the past from aircraft, and recently from the spacecraft STARDUST [*Brownlee et al.*, 2006] in the coma of the comet P81/Wild2. The relative velocity between the collecting devices and the surrounding medium are at least a few tens of meters per second and 6 km per second respectively, leads to partly destroying the particles if they have a high porosity. A new instrument, DUSTER, is under development at the University of Napoli (Italia), and is planned to be mounted on some of our gondolas in near future (P. Palumbo, personal communication, 2007). Since the stratospheric balloon is carried by the wind, the relative velocity between the gondola and the surrounding particles is small. The only relative motion of the gondola is a swaying under the flight chain and this was found to be smaller than 0.5 m s^{-1} during the previous SALOMON flights. Preliminary tests in the laboratory show that DUSTER has an optimal working range for the collection of particles having sizes between 0.1 and 1 μm, and that larger particles can be collected but with lower efficiency.

[70] Establishing a global climatology of the vertical and latitudinal repartition of the various families of aerosols will allow us to distinguish between droplets, soot and interplanetary grains. It will allow us also to better document the occurrence of middle and upper stratosphere enhancements of nonterrestrial material, thus better estimating its average amount in the atmosphere. After the preliminary climatology of the global content of stratospheric aerosols already performed using the 2003 GOMOS observations [*Vanhellemont et al.*, 2005], this will be done in the near future using all the GOMOS measurements performed since its launch in 2002 by using the LPCE processor for the retrievals. Only the GOMOS occultations performed using the brightest stars will be considered in order to have a high signal-to-noise ratio for retrieving unambiguously the wavelength dependence of aerosol extinction.

[71] Finally, new balloon flights of STAC, SALOMON, MicroRADIBAL and DUSTER are expected to be performed from 2009 during national and European campaigns. These new measurements will be compared to the GOMOS measurements (expected to continue up to 2013) if the spatial and temporal collocation is good, in order to check the accuracy of the GOMOS products used for establishing the aerosol climatology. They will also help to better document the trend of the soot content in the stratosphere and its possible but unexplained spatial variability. These new satellite and balloon-borne results will the subject of a second paper.

[72] **Acknowledgments.** The MicroRADIBAL, SALOMON and STAC flights were funded by the CNES and ESA during a validation program of Envisat. The authors want to thank the CNES launching team for the success of the flights, and the reviewers for their useful comments. J. Ovarlez, H. Ovarlez, V. Catoire, P. Palumbo and G. Ancellet are acknowledged for their helpful discussions. The "Palais de la Découverte" is thanked for its logistic support.

References

Baumgardner, D., G. Kok, and G. Raga (2004), Warming of the Arctic lower stratosphere by light absorbing particles, *Geophys. Res. Lett.*, *31*, L06117, doi:10.1029/2003GL018883.

Bemer, D., J. F. Fabries, and A. Renoux (1990), Calculation of the theoretical response of an optical particle counter and its practical usefulness, *J. Aerosol Sci.*, *21*, 689–700, doi:10.1016/0021-8502(90)90123-F.

Bertaux, J.-L., et al. (2004), First results on GOMOS/ENVISAT, *Adv. Space Res.*, *33*, 1029–1035, doi:10.1016/j.asr.2003.09.037.

Berthet, G., J.-B. Renard, C. Brogniez, C. Robert, M. Chartier, and M. Pirre (2002), Optical and physical properties of stratospheric aerosols from balloon measurements in the visible and near-infrared domains. I. Analysis of aerosol extinction spectra from the AMON and SALOMON balloonborne spectrometers, *Appl. Opt.*, *41*, 7522–7539, doi:10.1364/AO.41.007522.

Berthet, G. (2007), Remote sensing measurements in the polar vortex: Implications for the simultaneous retrievals and analysis of the NO_2 and OClO species, *J. Geophys. Res.*, *112*, D21310, doi:10.1029/2007JD008699.

Biermann, U. M., T. Presper, T. Koop, J. Mößinger, P. J. Crutzen, and T. Peter (1996), The unsuitability of meteoritic and other nuclei for polar stratospheric cloud freezing, *Geophys. Res. Lett.*, *23*, 1693–1696, doi:10.1029/96GL01577.

Bingen, C., D. Fussen, and F. Vanhellemont (2004), A global climatology of stratospheric aerosol size distribution parameters derived from SAGE II data over the period 1984–2000: 2. Reference data, *J. Geophys. Res.*, *109*, D06202, doi:10.1029/2003JD003511.

Blake, D. F., and K. Kato (1995), Latitudinal distribution of black carbon soot in the upper troposphere and the lower stratosphere, *J. Geophys. Res.*, *100*, 7195–7202, doi:10.1029/94JD03118.

Brogniez, C., N. Huret, S. Eckermann, E. D. Rivière, M. Pirre, M. Herman, J.-Y. Balois, C. Verwaerde, N. Larsen, and B. Knudsen (2003), PSC microphysical properties measured by MicroRADIBAL instrument on January 25, 2000 above Esrange and modeling interpretation, *J. Geophys. Res.*, *108*(D6), 8332, doi:10.1029/2001JD001017.

Brownlee, D. (1985), Cosmic dust: Collection and research, *Annu.Rev. Earth Planet. Sci.*, *13*, 147–173, doi:10.1146/annurev.ea.13.050185.001051.

Brownlee, D., et al. (2006), Comet 81P/Wild 2 under a microscope, *Science*, *314*, 1711–1716, doi:10.1126/science.1135840.

Curtius, J., et al. (2005), Observations of meteoric material and implications for aerosol nucleation in the winter Arctic lower stratosphere derived from in situ particle measurements, *Atmos. Chem. Phys.*, *5*, 3053–3069.

Cziczo, D. J., D. S. Thomson, and D. M. Murphy (2001), Ablation, flux and atmospheric implication of meteors inferred from stratospheric aerosols, *Science*, *291*, 1772–1775, doi:10.1126/science.1057737.

Damoah, R., N. Spichtinger, R. Servranckx, M. Fromm, E. W. Eloranta, I. A. Razenkov, P. James, M. Shulski, C. Forster, and A. Stohl (2006), A case study of pyro-convection using transport model and remote sensing data, *Atmos. Chem. Phys.*, *6*, 173–185.

Deshler, T., M. E. Hervig, D. J. Hofmann, J. M. Rosen, and J. B. Liley (2003), Thirty years of in situ stratospheric aerosol size distribution measurements from Laramie, Wyoming (41°N) using balloon-borne instruments, *J. Geophys. Res.*, *108*(D5), 4167, doi:10.1029/2002JD002514.

Di Girolamo, P., G. Pappamardo, N. Spinelli, V. Berardi, and R. Velotta (1996), Lidar observations of the stratospheric aerosol layer over southern Italy in the period 1991–1995, *J. Geophys. Res.*, *101*, 18,765–18,773, doi:10.1029/96JD01172.

Duprat, J., C. Engrand, M. Maurette, G. Kurat, M. Gounelle, and C. Hammer (2007), Micrometeorites from central Antarctic snow: The CONCORDIA collection, *Adv. Space Res.*, *39*, 605–611, doi:10.1016/j.asr.2006.05.029.

Dutton, E. G., P. Reddy, S. Ryan, and J. J. DeLuisi (1994), Features and effects of aerosol optical depth observed at Mauna Loa, Hawaii: 1982–1992, *J. Geophys. Res.*, *99*, 8295–8306, doi:10.1029/93JD03520.

Engrand, C., and M. Maurette (1998), Carbonaceous micrometeorites from Antarctica, *Meteorit. Planet. Sci.*, *33*, 565–580.

Fromm, M., and R. Servranckx (2003), Transport of forest fire smoke above the tropopause by supercell convection, *Geophys. Res. Lett.*, *30*(10), 1542, doi:10.1029/2002GL016820.

Fussen, D., F. Vanhellemont, and C. Bingen (2001), Remote sensing of the Earth's atmosphere by the spaceborne occultation radiometer ORA: Final inversion algorithm, *Appl. Opt.*, *40*, 941–948, doi:10.1364/AO.40.000941.

Gerding, M., G. Baumgarten, U. Blum, J. P. Thayer, K.-H. Fricke, R. Neuber, and J. Fiedler (2003), Observation of an unusual mid-stratospheric aerosol layer in the Arctic: Possible sources and implication for polar vortex dynamics, *Ann. Geophys.*, *21*, 1057–1069.

Hanson, D. R., A. R. Ravishankara, and S. Solomon (1994), Heterogeneous reactions in sulphuric acid aerosols: A framework for model calculation, *J. Geophys. Res.*, *99*, 3615–3629, doi:10.1029/93JD02932.

Hanson, D. R., A. R. Ravishankara, and E. R. Lovejoy (1996), Reactions of $BrONO_2$ with H_2O on submicron sulphuric acid aerosol and implication for the lower stratosphere, *J. Geophys. Res.*, *101*, 9063–9069, doi:10.1029/96JD00347.

Heald, C. L., et al. (2006), Concentrations and sources of organic carbon aerosols in the free troposphere over North America, *J. Geophys. Res.*, *111*, D23S47, doi:10.1029/2006JD007705.

Hendricks, J., B. Kärcher, A. Döpelheuer, J. Feichter, U. Lohmann, and D. Baumgardner (2004), Simulating the global atmospheric black carbon cycle: A revisit to the contribution of aircraft emission, *Atmos. Chem. Phys.*, *4*, 2521–2541.

Herman, M., J.-Y. Balois, L. Gonzales, P. Lecomte, J. Lenoble, R. Santer, and C. Verwaerde (1986), Stratospheric aerosol observations from a balloon-borne polarimetric experiment, *Appl. Opt.*, *25*, 3573–3584.

Hervig, M. E., and T. Deshler (1998), Stratospheric aerosol surface area and volume inferred from HALOE, CLAES, and ILAS measurements, *J. Geophys. Res.*, *103*, 25,345–25,352, doi:10.1029/98JD01962.

Hovenier, J. W., H. Volten, O. Muñoz, W. J. van der Zande, and L. B. Waters (2003), Laboratory studies of scattering matrices for randomly oriented particles: Potentials, problems, and perspectives, *J. Quant. Spectrosc. Radiat. Transfer*, *79–80*, 741–755, doi:10.1016/S0022-4073(02)00319-9.

Hunten, D. M., R. P. Turco, and O. B. Toon (1980), Smoke and dust particles of meteoric origin in the mesosphere and stratosphere, *J. Atmos. Sci.*, *37*, 1342–1356, doi:10.1175/1520-0469(1980)037<1342:SADPOM>2.0.CO;2.

Jäger, H., O. Uchino, T. Nagai, T. Fujimoto, V. Freudenthaler, and F. Homburg (1995), Ground-based remote sensing of the decay of the Pinatubo eruption cloud at three Northern Hemisphere sites, *Geophys. Res. Lett.*, *22*, 607–610, doi:10.1029/95GL00054.

Jessberger, E. K. (1999), Rocky cometary particles: Their elemental, isotopic and mineralogical ingredients, *Space Sci. Rev.*, *90*, 91–97, doi:10.1023/A:1005233727874.

Jost, H.-J., et al. (2004), in-situ observations of mid-latitude forest fire plumes deep in the stratosphere, *Geophys. Res. Lett.*, *31*, L11101, doi:10.1029/2003GL019253.

Klekociuk, A., P. G. Brown, D. W. Pack, D. O. ReVelle, W. N. Edwards, R. E. Spalding, E. Tagliaferri, B. B. Yoo, and J. Zagari (2005), Meteoritic dust from the atmospheric disintegration of a large meteoroid, *Nature*, *436*, doi:10.1038/nature03881.

Kyrölä, E., et al. (2004), GOMOS on Envisat: An overview, *Adv. Space Res.*, *33*, 1020–1028, doi:10.1016/S0273-1177(03)00590-8.

Lary, D. J., D. E. Shallcross, and R. Toumo (1999), Carbonaceous aerosols and their potential role in atmospheric chemistry, *J. Geophys. Res.*, *104*, 15,929–15,940, doi:10.1029/1998JD100091.

Love, S. G., and D. E. Brownlee (1993), A direct measurement of the terrestrial mass accretion rate of cosmic dust, *Science*, *262*, 550–553, doi:10.1126/science.262.5133.550.

Maurette, M., C. Olinger, M. Michel-Levy, G. Kurat, M. Pourchet, F. Brandstätter, and M. Bourot-Denise (1991), A collection of diverse micrometeorites recovered from 100 tons of Antarctic blue ice, *Nature*, *351*, 44–47, doi:10.1038/351044a0.

Mishchenko, M. I., L. D. Travis, and D. W. Mackowski (1996), T-matrix computations of light scattering by nonspherical particles: A review, *J. Quant Spectrosc. Radiat. Transfer*, *55*, 535–575, doi:10.1016/0022-4073(96)00002-7.

Moulin, F. (2007), Modélisation morphologique des suies émises par les avions, Ph.D. thesis, France-Comté Univ., Besançon, France.

Murphy, D. M., D. S. Thomson, and M. J. Mahoney (1998), In situ measurements of organics, meteoritic material, mercury, and other elements in aerosols at 5 to 19 kilometers, *Science*, *282*, 1664–1669, doi:10.1126/science.282.5394.1664.

Murphy, D. M., D. J. Cziczo, P. K. Hudson, and D. S. Thomson (2007), Carbonaceous material in aerosol particles in the lower stratosphere and tropopause region, *J. Geophys. Res.*, *112*, D04203, doi:10.1029/2006JD007297.

Ovarlez, J., and H. Ovarlez (1995), Water vapour and aerosol measurements during SESAME, and the observation of low water vapour content layers, in *Polar Stratospheric Ozone*, edited by J. A. Pyle, N. R. P. Harris, and G. T. Amanatidis pp. 205-208, Eur. Comm., Brussels.

Platt, U. (1994), Differential optical absorption spectroscopy (DOAS), in *Air Monitoring by Spectroscopic Techniques*, *Chem. Anal. Ser.*, vol. 127, pp. 27–83, John Wiley, Hoboken, N. J.

Pusechel, R. F., D. F. Blake, K. G. Snetsinger, A. D. A. Hansen, S. Verma, and K. Kato (1992), Black carbon (soot) in the lower stratosphere and upper troposphere, *Geophys. Res. Lett.*, *19*, 1659–1662, doi:10.1029/92GL01801.

Pueschel, R. F., K. A. Boering, S. Verma, S. D. Howard, G. V. Ferry, J. Goodman, D. A. Allen, and P. Hamill (1997), Soot aerosol in the lower stratosphere: Pole-to-pole variability and contributions by aircraft, *J. Geophys. Res.*, *102*, 13,113–13,118, doi:10.1029/96JD03061.

Pueschel, R. F., S. Verma, H. Rohatschek, G. V. Ferry, N. Boiadjieva, S. D. Howard, and A. W. Strawa (2000), Vertical transport of anthropogenic soot aerosol into the middle atmosphere, *J. Geophys. Res.*, *105*, 3727–3736, doi:10.1029/1999JD900505.

Quirantes, A. (2005), A T-matrix method and computer code for randomly oriented, axially symmetric coated scatterers, *J. Quant. Spectrosc. Radiat. Transfer*, *92*, 373–381, doi:10.1016/j.jqsrt.2004.08.004.

Ray, E. A., et al. (2004), Evidence of the effect of summertime midlatitude convection on the subtropical lower stratosphere from CRYSTAL-FACE tracer measurements, *J. Geophys. Res.*, *109*, D18304, doi:10.1029/2004JD004655.

Renard, J.-B., E. Hadamcik, C. Brogniez, G. Berthet, J.-C. Worms, M. Chartier, M. Pirre, J. Ovarlez, and H. Ovarlez (2001), UV-visible bulk optical properties of randomly distributed soot, *Appl. Opt.*, *40*, 6575–6580, doi:10.1364/AO.40.006575.

Renard, J.-B., et al. (2002), Optical and physical properties of stratospheric aerosols from balloon measurements in the visible and near-infrared domains: II. Comparison of extinction, reflectance, polarization and counting measurements, *Appl. Opt.*, *41*, 7540–7549, doi:10.1364/AO.41.007540.

Renard, J.-B., J. Ovarlez, G. Berthet, D. Fussen, F. Vanhellemont, C. Brogniez, E. Hadamcik, M. Chartier, and H. Ovarlez (2005a), Optical and physical properties of stratospheric aerosols from balloon measurements in the visible and near-infrared domains. III. Presence of aerosols in the middle stratosphere, *Appl. Opt.*, *44*, 4086–4095, doi:10.1364/AO.44.004086.

Renard, J.-B., D. Daugeron, P. Personne, G. Legros, J. Baillargeat, E. Hadamcik, and J.-C. Worms (2005b), Optical properties of randomly distributed soot–improved polarimetric and brightness scattering functions, *Appl. Opt.*, *44*, 591–596, doi:10.1364/AO.44.000591.

Renard, J.-B., et al. (2008), Validation of GOMOS-Envisat vertical profiles of O_3, NO_2, NO_3, and aerosol extinction using balloon-borne instruments, *J. Geophys. Res.*, *113*, A02302, doi:10.1029/2007JA012345.

Rohatschek, H. (1996), Levitation of stratospheric and mesospheric aerosols by gravito-photophoresis, *J. Aerosol Sci.*, *27*, 467–475, doi:10.1016/0021-8502(95)00556-0.

Russell, P. B., et al. (1996), Global to microscale evolution of the Pinatubo volcanic aerosol derived from diverse measurements and analyses, *J. Geophys. Res.*, *101*, 18,745–18,763, doi:10.1029/96JD01162.

Santer, R., M. Herman, D. Tanré, and J. Lenoble (1988), Characterization of stratospheric aerosol from polarization measurements, *J. Geophys. Res.*, *93*, 14,209–14,221, doi:10.1029/JD093iD11p14209.

Schwarz, J. P., et al. (2006), Single-particle measurements of mid-latitude black carbon and light-scattering aerosols from the boundary layer to the lower stratosphere, *J. Geophys. Res.*, *111*, D16207, doi:10.1029/2006JD007076.

SPARC (2006), Assessment of stratospheric aerosols properties, *WMO/TD1295*, World Meteorol. Org., Geneva.

Steele, H. M., J. D. Lumpe, R. P. Turco, R. M. Bevilacqua, and S. T. Massie (1999), Retrieval of aerosol surface area and volume densities from ex-

tinction measurements: Application to POAM II and SAGE II, *J. Geophys. Res.*, *104*, 9325–9336, doi:10.1029/1999JD900032.

Strawa, A. W., et al. (1999), Carbonaceous aerosol (soot) measured in the lower stratosphere during POLARIS and its role in stratospheric photochemistry, *J. Geophys. Res.*, *104*, 26,753–26,766, doi:10.1029/1999JD900453.

VanderWood, T. B., M. Maurette, J. P. Bradley, C. Engrand, G. Kurat, J. R. Petit, and N. I. Barkov (1996), Automated SEM analysis of fine grained dust from Antarctica ice cores, *Lunar Planet. Sci.*, *XXXVII*, 1355–1356.

Vanhellemont, F., et al. (2005), A 2003 stratospheric aerosol extinction and PSC climatology from GOMOS measurements on Envisat, *Atmos. Chem. Phys.*, *5*, 2413–2417.

Zolensky, M. E., T. L. Wilson, F. J. M. Rietmeijer, and G. J. Fynn (1994), *Analysis of Interplanetary Dust*, Am. Inst. of Phys., New York.

F. Auriol, J.-Y. Balois, C. Brogniez, P. Francois, and C. Verwaerde, Université des Sciences et Technologies de Lille, LOA, CNRS, F-59655 Villeneuve d'Ascq CEDEX, France.

G. Berthet, M. Chartier, D. Daugeron, B. Gaubicher, and J.-B. Renard, LPCE CNRS, Université d'Orléans, 3A Avenue de la Recherche Scientifique, F-45071 Orléans, France. (jbrenard@cnrs-orleans.fr)

Q. Bourgeois, EPFL, LMCA, Station 2, CH-1015 Lausanne, Switzerland.

C. Engrand, CSNSM, CNRS IN2P3, Bâtiment 104, F-91405 Orsay, France.